The role of network structure in the central nervous control of caterpillar crawling and casting

A Senior Honors Thesis
by Elise Ewing

Tufts year 2012 – 2013

Abstract

Through numerical simulation, this study aims to understand a neuronal network that could be responsible for controlling several different behaviors of the caterpillar *Manduca sexta*, in hopes that the knowledge gained will be applicable to crawling in other caterpillars and soft-bodied units in general. Knowledge from previous studies has been compiled in order to determine target output patterns for our networks. Qualitatively, the crawling pattern consists of a slow posterior to anterior propagating wave of bursts of activity within the ganglia of the abdominal body segments in *Manduca*. Another behavior that we consider is casting, which is a side-to-side motion believed to be a searching behavior. This behavior is characterized by laterally anti-synchronous bursting within a ganglion that is concurrent in successive posterior and anterior ganglia. One side of the caterpillar is active, and then the other. Working from simple feasible network designs, simulations were run in order to determine parameter regimes where our network could produce different desired outputs. We have found that a bilateral network of inhibitory neurons with adaptation currents can produce either synchronous or anti-synchronous behavior when stimulated under different initial conditions. We have also found that the slow anterior propagating wave of the crawling pattern can be produced in a network of anterior linked excitatory neurons if those neurons release neurotransmitter that persists for a relatively long time in the synapse, and each neuron is self-inhibited by an adaptation current that acts on an even slower time scale.

1 Introduction

Neuroscience, whether it is being approached from a biological, mathematical, or computational point of view can be thought of as asking questions about control. The central nervous system (CNS) allows an organism to sense and perceive the world around it and to control its motions in order to interact. The basic unit of the CNS is the neuron. How neurons are used to transfigure sensory inputs into motor outputs is determined by the structure of the nervous system and the functionality of individual neurons. Scientists run into problems trying to study the CNS of *Manduca sexta* because it is small. Other model organisms, with larger neurons and fewer synapses, could provide more data for modeling. We chose *Manduca* because its completely non-rigid body produces consistent rhythmic locomotion. Mathematicians have developed tools that allow us to approach the problem from a different angle while still modeling the control system like a network of neurons. If we think of the CNS more abstractly, we can use mathematical neuron models to answer questions that we have about the capacity of different configurations of theoretical neurons, or to develop hypotheses about how the CNS may be comprised.

Consider any system that transfers information. There is some quantity that is the information, and another that is the structure through which the information is transported. Within the nervous system, the action potential (AP) and the temporal pattern of APs is the information, and the network connectivity of neurons, or unit AP producers, is the transportation structure. The output of an individual neuron is the answer to the yes or no question, "Am I firing an AP or not?" The question is asked at every instant in time and the answers, or rate of 'yes' answers, make this temporal pattern. The output or the message that is communicated by the network is not only the temporal pattern of APs but which neurons are firing them. Thus, a network can communicate much more information than one neuron firing an all-or-nothing signal. It is sort of like considering the electricity through one stretch of copper wire rather than the functioning of an entire microchip or computer.

To illustrate this idea, consider the example of the human hand. We could not clench our fists if the muscles controlling our fingers did not contract. However, it is the morphological advantage of the opposable thumb that allows us to pick up, grab on, and grasp in such a wide variety of ways. The information here is the muscle contraction. The transportation structure of the hand produces the fine tuned behavior from the information input. In this way much of the control of our motions is encoded in or embodied by the structure of the hand. The idea that some of the knowledge or intelligence exists in the structure or tissues of a body, not the nervous system, is referred to as embodied intelligence and has been of growing interest in the computer science, robotics, artificial intelligence, and biology communities lately (For an in depth discussion of embodied control see Pfeifer and Bongard 2007, Ch. 1 & 2).

The idea of embodied control can be applied to the CNS. The configuration of a network can embody the control of a behavior. The topic of the locus of control within the nervous system

has been a source of debate within the neuroscience community. Two hypotheses about where the control of behavior originates are present; one is much more congruent with the idea of embodied control. One, the "command neuron" hypothesis, argues that it is possible to locate one neuron in a network that is "necessary and sufficient" to produce a behavior (Delcomyn 1980). The other is the idea of a central pattern generator, or CPG. The network structure of a CPG gives rise to a self-sustaining output pattern that dictates the time course of rhythmic behaviors. So, control is embodied by the connectivity of the network, not any one individual neuron. Evidence for CPG control crawling in *Manduca* (Johnston and Levine 1996), walking in the locust (Kien 1983, Ryckebusch and Laurent 1993), feeding in *Drosophila* (Gorczyca et al. 1991), and chewing in the gut of the lobster (Selverston et al. 1976). It is very plausible that both ideas about control, command neurons and CPGs, are found in living nervous systems. A command neuron could initiate or alter the activity of a CPG, or CPGs on a higher level of control.

Using numerical models, we aim to determine which components of a neuronal network that would be plausible in *Manduca sexta* can allow it to act as a central pattern generator to produce output patterns reminiscent of both the caterpillar's crawling and casting behaviors. In the future we hope that the information we gather can assist as Tufts Neuromechanics and Biomimetic Devices laboratory moves towards controlling a bio-actuated and bio-fueled soft-bodied robot. The interplay of neural and embodied control is especially important with a caterpillar model system because the lack of hard parts gives rise to uncountable degrees of freedom that must be coordinated to produce behavior. We work towards understanding what each neuron in the network must incorporate and how the neurons must be connected in order to produce desired output patterns. The task of modeling has been broken up into two parts. In the larva of *Manduca sexta* an anterior grade wave of activity in the CNS is believed to produce the crawling behavior, and a laterally anti-synchronous pattern is believed to produce the casting behavior. First a simplified nerve cord is studied to understand the slow forward propagation of a wave of activity in the CNS that is believed to control crawling. Second, a laterally anti-synchronous pattern that could give rise to the casting behavior within an individual ganglion network is studied separately. We hypothesize that in both cases the addition of an adaptation current to act as self inhibition within the neurons will be necessary to produce our desired results. *Manduca sexta* is the species that we concentrate on, but we do hope that the work will be applicable to describing caterpillars and soft bodied units in general.

2 Biological background

To begin the our modeling process, we considered a simplified caterpillar. This caterpillar is a soft cylinder with ends designated as the head and tail. The body is divided into segments or units. In total *Manduca* has twelve body segments; a terminal segment, seven abdominal

segments, three thoracic segments and a head. For a very accurately drawn picture of the $5th$ instar larvae of *Manduca* see Figure 1. We consider the abdominal segments and ignore the prolegs and components thereof (added musculature for retraction, etc.), and take all segments to be functionally identical. The body wall is connected to a muscular system that is controlled by the CNS. (For details see Levine and Truman 1985.) In general, muscles cause a segment to contract in a particular direction, and the level of recruitment of individual muscles combined is what produces a particular behavior.

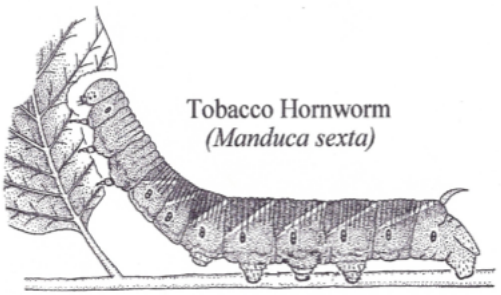

Figure 1: **Fifth instar larvae of *Manduca sexta*.** Accurately drawn diagram reproduced from Patton 2000, FIG. 1

The central nervous system of *Manduca sexta* is organized into the nerve cord, which runs along the ventral midline on the interior of the cuticle (Lane 1972, Morris 1984, and Pichon et al. 1972). The nerve cord is structured such that there are places where many neuron cell bodies and their local synapses come together, called ganglia, with stretches of longer axons in between. Ganglia look like knots in the rope that is the nerve cord. Each segment has a corresponding ganglion, and each ganglion receives afferent sensory information and sends efferent control signals to the tissues.

Interneurons facilitate the connection between sensory and motor neurons, but their presence is not necessary in all cases. Reflexes that do not involve interneurons can be advantageous in situations where a fast response is necessary. In defensive situations, for example, organisms have evolved monosynaptic reflex pathways to facilitate quick escapes. One example of this is the proleg withdrawal reflex in *Manduca*. When sensory hairs at the tip of the proleg are bent the reflex is evoked through a monosynaptic pathway and the proleg is retracted back into the body (Weeks and Jacobs 1987, Mezoff et al. 2004). However, usually interneurons facilitate connections within the CNS, playing a computational role. They process and distribute the information they receive from sensory inputs, which is often used to send appropriate signals to produce motor outputs. Interneurons can also work together in networks of different configurations. In their 1987 work, Torre and Poggio present a discussion of different mechanisms or networks proposed to determine directional selectivity within visual systems of different species (Torre and Poggio 1978). Also, interneuron networks that produce patterned output when they receive a sensory stimulus, or central pattern generators (CPGs), are widely studied. Behaviors such as ecdysis (Weeks and Truman 1984) and pre-ecdysis (Novicki and Weeks 1995) in *Man-*

duca are believed to be produced by CPGs. Swimming in the marine mollusk (Getting 1981), chewing in the gut of the lobster (Selverston et al. 1976), and many other behaviors patterns are centrally generated as well.

The extreme detail and small size of the CNS in *Manduca* make it difficult for researchers to gain an accurate picture of the connections between, or even number of, interneurons it contains. Researchers have been able to gain some picture of motor patterns within *Manduca* because they have recorded from sensory neurons and motor neurons.

For this study, we have taken advantage of the phenomenon of *fictive behavior patterns*. A fictive behavior pattern is a pattern that qualitatively looks like a the motor output that would drive a behavior in the living organism, but is produced in a reduced preparation. In these experiments, the nerve cord is completely isolated which means that there is no sensory feedback. Through the application of specific drugs, *fictive* behavior patterns have been observed in many organisms. Due to the similarity, the pattern is believed to be produced by the same network that produces the behavior in the living creature. In theory, the applied drug acts like whatever nervous trigger is present in the living nervous system to start the behavior pattern, and since the nervous structure is still present *in vitro* the output pattern is still observable. Even if not much is known about the CNS structure of a given organism, if a fictive behavior can be observed, it provides strong evidence for CPG control of that behavior. A *fictive chewing* pattern was observed in the subesophageal ganglion of *Manduca* (Rohrbacher 1994). The application of the muscarinic agonist pilocarpine evoked a fictive feeding pattern in *Drosophila* (Gorczyca et al. 1991), and a fictive walking pattern in the locust (Ryckebusch and Laurent 1993). Fictive locomotion has been observed in the lamprey (Cohen and Harris-Warrick 1984) We have studied *fictive crawling* in *Manduca* in order to learn the details of the crawling pattern that we would like our networks to produce. Fictive crawling is produced when the isolated nerve cord when it is exposed to pilocarpine. Much work on the study of fictive crawling in *Manduca* has been performed by Rebecca Johnston and Richard Levine (Johnston and Levine 1996, Johnston et al. 1998, Johnston and Levine 2002). The pattern is most often recorded at the extra cellular level, so the activity within nerves, but not specific motor neurons within those nerves, is recorded. Data from a pilocarpine bath study published by Johnston and Levine is reproduced in Figure 2. Also, the similarity between fictive crawling and the believed crawling motor pattern is qualitative but not quantitative in that crawling *in vivo* occurs about 2.5 times faster than fictive crawling (*in vitro*) (Johnston and Levine 1996, Simon et al. 2010), similar to the locust (Ryckebusch and Laurent 1993). In *fictive crawling* the burst duration within a ganglion is 8 to 9 seconds. The latency between the onset of bursting in one ganglion and the next anterior ganglion is slightly greater than one second, as is the offset latency. These numbers are estimated from measurements made from Figure 2. We were unable to determine the frequency of firing within the bursts from this figure.

In his senior thesis work, a Tufts student, Joe Patton, also tried to elicit the fictive crawling pattern in *Manduca* (Patton 2000). He was successful and also observed a new pattern that he

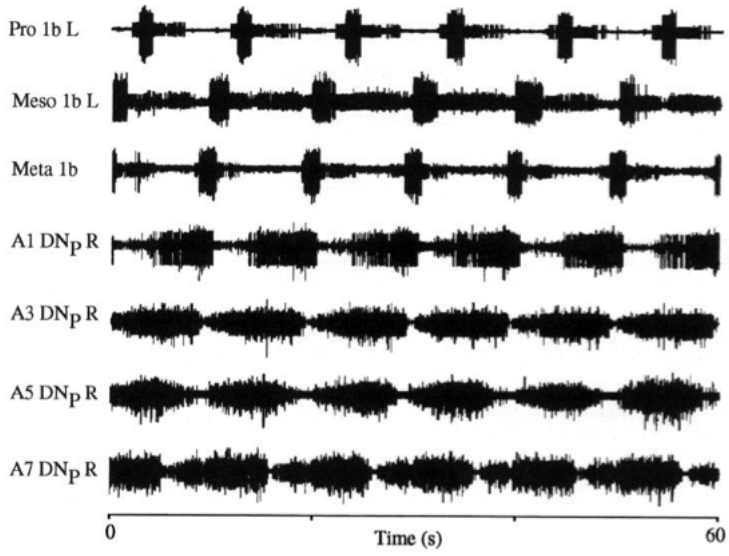

Figure 2: **Fictive crawling in *Manduca sexta*.** Spontaneous activity of neurons in the posterior branch of the dorsal nerve in abdominal ('A') and thoracic ('Meta', 'Meso', 'Pro') ganglia of *Manduca sexta* recorded from a reduced preparation during bath application of 1.0 mM pilocarpine. These data are reproduced from Johnston and Levine 1996, FIG. 6

deemed the *novel rhythm*. The novel rhythm is comprised of a laterally anti-synchronous but longitudinally synchronous output pattern. In other words, in all the ganglia along the nerve cord the motor neurons on one side are active simultaneously while those on the other are silent, and then the two sides reverse and the pattern repeats (Patton 2000). These neurons synapse on the muscles that control the body wall (Levine and Truman 1985). This suggests that the novel rhythm could control an observed defensive or searching behavior called casting. When casting the animal moves laterally from one side to the other while all but its rear-most legs are elevated off of the substrate. For this reason, I will refer to Pattons novel rhythm as *fictive casting* from now on.

Two patterns emerging from the same experimental preparation posed an interesting question. Is it really the same network producing both of these behaviors, or are the two produced separately with output into the same nerve? We aim to determine what is important for the production of each behavior. We started with a goal network and made simplified versions that allow us to study one type of output at a time. The network that we started with (Figure 3) was first proposed by Joe Patton as a possible mechanism for creating both of the output patterns (Patton 2000, p. 23). We are concerned with the interneurons shown here (not MNs). This network is comprised of two sides (laterally) that are in competition. If one of the excitatory cells (E cells) fires, it excites inhibition which inhibits the firing of both of the cells on the other side of the network. In this we would expect that we could see laterally anti-synchronous patterns if one E cell were excited more than the other. Whereas if the two E cells fired equally they would both excite their corresponding inhibitory neurons and these neurons would inhibit one another. The idea would be that the synaptic strengths could be modified such that the

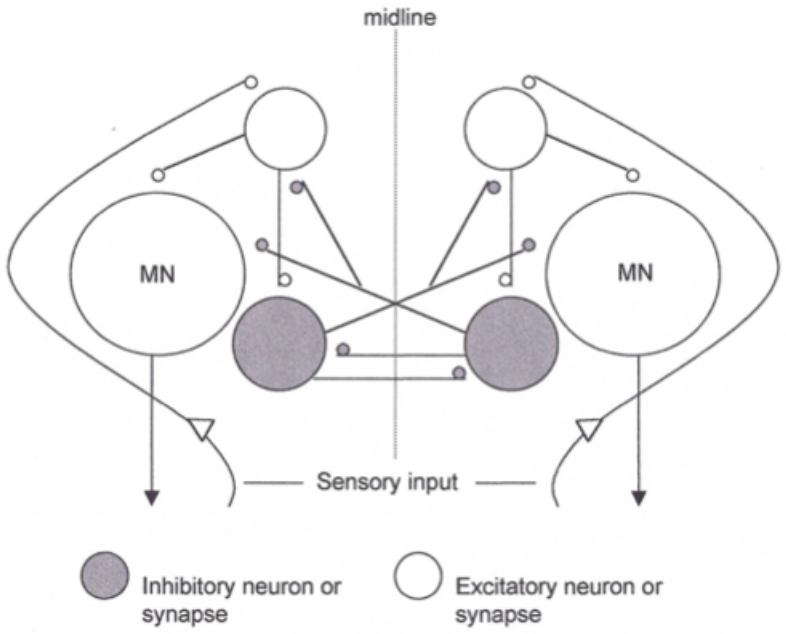

Figure 3: **Theoretical neuronal network within *Manduca* ganglia.** Network configuration capable of producing crawling and casting behavior in *Manduca* proposed by Joe Patton (Patton 2000, FIG. 8)

inhibition in this case would not cause both sides of the network to completely stop firing, but fire more infrequently, if they start firing together. Here we would expect to see laterally synchronous behavior. The purpose of our first set of experiments is to examine the conditions necessary for a nerve cord of simple excitatory ganglia to produce a slow crawling propagation pattern. The purpose of our second set of experiments is to test the capability of a simplified ganglion network model to determine whether the laterally competitive arrangement can produce both laterally synchronous and anti-synchronous patterns. Later, these two simplified networks could be combined, where each ganglion looks like Figure 3 and there are excitatory connections between them.

3 Mathematical background

Two different mathematical models of neurons were used in our simulations, the Linear Integrate and Fire model, and the Morris-Lecar Model. As discussed in the introduction, these and other model neurons have been used in many studies, both to test the capabilities of network configurations (ex. Lajoie and Shea-Brown 2011) and of individual neuronal models (ex. Av-Ron et al. 1991). In this section we will describe the two models and explain why each was chosen for its respective experiments.

3.1 Linear Integrate and Fire neuron model

The Linear Integrate and Fire (LIF) neuron is arguably the simplest of the mathematical neuron models. Biologists will probably object that LIF neurons are far too simple. However, we argue that the goal of modeling is to simplify the problem. Once a model is understood, it can be made more complex. In this way, we can understand how complex a model needs to be to accurately depict a problem, and in this gain understanding of the complexity of the problem itself. We believe that the essence of the forward propagating crawling pattern in *Manduca sexta* can be accurately represented temporally, and therefore that LIF neurons will be sufficient for modeling.

In the linear integrate-and-fire model, membrane potential, denoted v, is modeled with a simple differential equation below threshold. Action potentials are modeled by a discontinuous reset where the membrane potential is set to a specified reset potential, v_{reset}, whenever v reaches a specified threshold potential, v_{thr}. We have taken v_{reset} to be 0 and v_{thr} to be 1. For this reason, v is a non-dimensionalized quantity; it represents a voltage abstractly, but not quantitatively. The only unit that has not been taken out of the model is time, so our simulation results do represent temporal patterns and events accurately.

Below threshold, the differential equation governing the membrane potential is

$$\frac{dv}{dt} = \frac{-v}{\tau} + I,$$

where τ is the membrane time constant, and I is the input that the cell receives. If the cell is driven only by an applied current I_{ext} the input is simply equal to this drive, $I = I_{\text{ext}}$. If we assume that all cells start with initial membrane potential $v(0) = 0$ then the membrane potential at a given time is

$$v(t) = \tau I(1 - e^{-t/\tau}),$$

$$\text{if } v(t-0) = 1 \text{ then } v(t+0) = 0.$$

The second statement describes the reset condition. The notation $t-0$ refers to the beginning of a time step, and $t+0$ refers to the end. If at the beginning of a time step v has reached 1, then it is reset to 0 so that this value will be used for calculation in the next time step. Since we can analytically calculate $v(t)$ we are also able to calculate the time at which a neuron will fire its first spike given a constant external drive, I_{ext}. Since we have assumed a zero initial condition for membrane potential, this can be interpreted as the period of spiking for the cell,

$$T = \tau \frac{\tau I}{\tau I - 1}.$$

This quantity is closely related to the frequency at which a cell fires. Usually the period and frequency are reciprocal of one another but because of the need for a unit conversion from period in milliseconds to frequency in Hertz the two are related by

$$f = \frac{1000}{T}.$$

Each cell also has associated with it a gating variable, s, which represents the cell's ability to drive another cell, or (very abstractly) neurotransmitter released by the cell. It's time course is governed by

$$\begin{aligned} \frac{ds}{dt} &= \frac{-s}{\tau_s} \\ \text{if } v(t-0) &= 1 \text{ then } s(t+0) = s(t-0) + \varepsilon_s(1 - s(t-0)) \end{aligned}$$

where τ_s is the gating variable time constant and determines how long the neurotransmitter persists in the synapse. The drive from one cell is not simply received by the post synaptic cell, or incorporated into the differential equation dv/dt, like an external drive. Instead it is incorporated as $I = I_s$ where

$$I_s = gs(v_{rev} - v).$$

Here g, the strength of the synapse between the two neurons, can take on value within the closed interval from zero to one. The reversal potential, v_{rev} for a current is the voltage at which there is no net flow of ions across the membrane. When the reversal potential is crossed, the direction of flow of the ion reverses, either from outward to inward or visa versa. For an excitatory cell the reversal potential is greater than the threshold potential and for an inhibitory cell it is less than the reset potential. Having $I = I_s$ models the input like an ion current, which is notably different from modeling an input like an external drive.

Finally, LIF cells can include a variable to model an adaptation current. The adaptation variable w is very similar to s in that

$$\begin{aligned} \frac{dw}{dt} &= \frac{-w}{\tau_w} \\ \text{if } v(t-0) &= 1 \text{ then } w(t+0) = w(t-0) + \varepsilon_w \end{aligned}$$

where τ_w dictates the time course of the decay of the adaptation. The adaptation is incremented whenever the cell fires by ε_w. Since, the adaptation current effects the membrane potential by adding the term $-w$ into the differential equation for v, it brings the membrane potential down whenever it grows. Thus, adaptation is one way which neurons can exhibit self inhibition. With adaptation,

$$\frac{dv}{dt} = \frac{-v}{\tau} + I - w.$$

Adaptation is not exactly modeled as a current, though in living cells the adaptation is a current. It is incorporated into the model as simply a value, whereas currents would appear in the form $I = gs(v_{\text{rev}} - v)$ if they represent an ion current across the membrane, or simply an external

applied current in Amperes.

3.2 Morris-Lecar neuron model

The neuron model created by Catherine Morris and Harold Lecar (Morris and Lecar 1981) is more complicated than the LIF neuron. It is a simplified version of the HH neuron (Hodgkin and Huxley 1952). This means that it models individual ion currents in order to produce a simulated AP. The ML neuron incorporates currents of two ions, potassium and calcium. The APs are calcium driven, they are "calcium spikes", whereas *Manduca* has sodium spikes (Pichon et al. 1972). We chose the ML model because the calcium spikes allow the model to very easily include a calcium-gated adaptation current. The trade between sodium spikes and calcium spikes was made for simplicitys sake. Even though this exchange makes the model slightly less accurate in terms of *Manduca sexta*, we still favor these results over those that could be achieved with LIF neurons because Morris-Lecar neurons (ML neurons) are more neuron-like or biologically accurate (cite the figure maybe include the figure).

The equations governing the membrane potential of a ML neuron follow. The exact equations given by Morris and Lecar in their 1981 work (Morris and Lecar 1981) have modified so that $M = M_\infty(v)$ always. They have also been written in the format that is consistent with the Simulator for Neural Networks and Action Potentials (SNNAP; ©1993-2003 The University of Texas Health Science Center at Houston, Houston TX, http://snnap.uth.tmc.edu) software package that we used to simulate ML neurons.

$$\begin{aligned} C\frac{dv}{dt} &= \overline{g}_K N(v_k - v) + \overline{g}_{Ca} M(v_{Ca} - v) - \overline{g}_L(v_L - v) + I \\ M &= M_\infty(v) \\ \frac{dN}{dt} &= \frac{N_\infty(v) - N}{\tau_N(v)} \end{aligned}$$

Here the subscript v represent the reversal potential for the ionic currents and the leak across the membrane, and the subscript $\overline{g}$ represent the maximum conductances for each of the currents. The quantity M represents the percentage of calcium gates that are open at a given point in time. Setting $M = M_\infty(v)$ means that we are assuming that these channels open instantaneously. This does not effect our modeling too adversely because these ion channels do open on a timescale that is much quicker (at least an order of magnitude) than the other processes within the model (like thes opening of the potassium gates). The quantity N represents the percentage of potassium gates that are open at a given time. This quantity is not assumed to

respond instantaneously to changes in voltage, as N is governed by a differential equation.

$$\begin{aligned} M_\infty(v) &= \frac{1}{1+e^{(-1.2-v)/9}} \\ N_\infty(v) &= \frac{1}{1+e^{(12-v)/8.7}} \\ \tau_N(v) &= \frac{0.008695}{e^{(v-12)/34.8}+e^{-(v-12)/34.8}} \end{aligned}$$

We performed experiments using a calcium gated potassium current for adaptation. When this current is incorporated into the model the term

$$\overline{g}_{K(Ca)}\frac{[Ca^{2+}]}{1+[Ca^{2+}]}(v_k - v)$$

is added to the right hand side of the differential equation governing the membrane potential.

One advantage of the ML model over the LIF model is that there is no discontinuous reset, which means that the ML model truly involves differential equations. This is nice for the sake of continuity. One disadvantage of the ML model is that there are many parameters. This means that searching the parameter space would take much longer than for a LIF neuron. We chose to start our parameter search using values that we knew would produce spiking. We took these values from the example Morris Lecar cell model that is included with the SNNAP software package for tutorial purposes. The numeric values in the equations for $M_\infty(v)$, $N_\infty(v)$, and $\tau_N(v)$ are specific to this source and can be replaced with different values when ML neurons are used in other contexts. They are related Morris and Lecar's parameters $v_1, ..., v_4$ (Morris and Lecar 1981).

$$\overline{g}_{Ca} = 0.2mS/cm^2 \qquad \overline{g}_K = 0.4mS/cm^2 \qquad \overline{g}_{k(Ca)} = 0.0125mS/cm^2 \qquad \overline{g}_L = 0.1mS/cm^2$$

$$C = 1\mu F/cm^2 \qquad v_{Ca} = 120mV \qquad v_K = -84mV \qquad v_{Ca} = -60mV$$

Synapses are modeled as a neurotransmitter gated current, I_{cs}, that is transferred from the pre- to the post-synaptic neuron. In the right hand side of the differential equation describing the membrane potential the term

$$I_{cs} = g(t)(v - v_{rev})$$

would be added. Where

$$\begin{aligned} g(t) &= \overline{g}A \\ \frac{d^2A}{dt^2} &= \frac{X - 2u(dA/dt) - A}{u^2} \\ X(t) &= \begin{cases} 1 & \text{pre-synaptic cell is firing} \\ 0 & \text{otherwise} \end{cases} \\ u &= 0.0031 \end{aligned}$$

A is the synaptic gating variable (s in the LIF model) and u is a time constant.

4 mAChR controlled sEPSP is a plausible mechanism for slow propagation

Slow conduction of signal from one ganglion to the next does not explain the speed of the crawling pattern because the conduction velocity of interneurons in *Manduca* is approximately half a meter per second (Novicki and Weeks 1995, Waldrop and Levine 1992, Sandstrom and Weeks 1991). We explored another possible mechanism. We looked for currents in *Manduca* that rose and decayed slowly. The slow rise meant that a driven neuron that incorporated this current would not start to fire the instant that it received drive while slow decay meant that the bursts would be relatively long in duration. We found a current deemed the "slow Excitatory Post Synaptic Potential" or sEPSP in *Manduca*'*s* PPR motoneuron (Trimmer and Weeks 1993, Trimmer 1994). We do realize that the properties of the interneurons in *Manduca* may vary significantly from those of the motoneurons, but we have chosen to overlook this detail because we do not have knowledge of any suitable currents in *Manduca* interneurons. This current has been thoroughly examined by Trimmer, who has discovered that it is a muscarinic ACh current that is carried primarily by sodium (Trimmer and Weeks 1993). Trimmer also has published data about the time course of this current, which is reproduced in Figure 4.

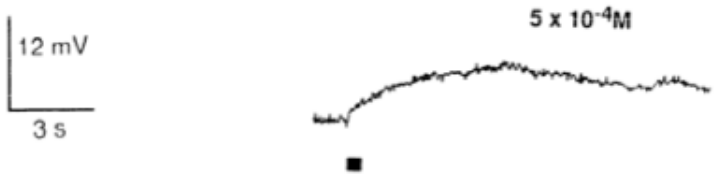

Figure 4: **Slow mAChR gated current in *Manduca*** Reproduced from Trimmer and Weeks 1993 FIG. 2. Slow excitatory post synaptic potential in the PPR motoneuron exposed to $5 \times 10^4 M$ mecamylamine, a nicotinic ACh receptor blocker, to suppress spiking. The black bar indicates the stimulus (50Hz 500ms) applied to the anterior branch of the ventral nerve which synapses on the PPR neuron.

We also found encouraging evidence of mAChR gated currents involved in other centrally

generated patterns and fictive behaviors (For review see Trimmer 1995). For example, the walking pattern in the locust can be evoked by bath application of pilocarpine in a reduced preparation and suppressed with atropine, which suggests that a necessary current is gated by mAChRs (Ryckebusch and Laurent 1993). Similar reaction to pilocarpine and atropine suggest that fictive feeding in *Drosophila* is aided by a mAChR gated current (Gorczyca et al. 1991).

We then wanted to determine whether Trimmer's mAChR gated sEPSP was a plausible mechanism for the slow propagation of the crawling motor pattern along the nerve cord. Considering only the ability of a ganglion to excite the next ganglion and to be excited by the previous ganglion, we represented our network model as a chain of E cells, each driving the next, and the last driving the first. Call it a circular chain of bursters. To put this model into the context of Patton's model (Figure 3), consider that we represented his entire network with one excitatory cell to simply model the output from one ganglion that would drive the next. We modeled the sEPSP in ganglion k as rising, reaching a plateau, and then decaying away. Ganglion k fired APs whenever it's membrane potential was higher than the threshold voltage, which we have taken to be $v_{\text{thr}} = 1$ for our LIF model. This activity drove ganglion $k+1$.

4.1 Abstract overview

Assume that ganglion k is active (fires) in time

$$[s_k, t_k].$$

We define

$$L_k = t_k - s_k.$$

Assume that

$$s_{k+1} = s_k + \delta_{\text{on}}, \quad t_{k+1} = t_k + \delta_{\text{off}}.$$

We assume that δ_{on} is fixed and given. This makes sense because we can calculate it. However, we assume that δ_{off} is a function of L_k. This reflects the idea that the activity of burst $k+1$ builds up an adaptation current, and the higher that current, the faster will the activity stop after burster k ceases to give input to burster $k+1$. So we assume that δ_{off} is a strictly decreasing function of L_k. So

$$L_{k+1} = L_k + \delta_{\text{off}}(L_k) - \delta_{\text{on}}.$$

We denote the right-hand side by $g(L_k)$. We will spell out conditions under which the equation

$$L_{k+1} = g(L_k)$$

has a solution, so g has a fixed point, and the fixed point is stable.

There is a fixed point if and only if there is a burst duration L for which

$$\delta_{\text{off}}(L) = \delta_{\text{on}}.$$

This is guaranteed to be true if δ_{off} depends on L continuously (a completely reasonable assumption), and $\delta_{\text{off}}(L) < \delta_{\text{on}}$ for large L (reflecting a sufficiently powerful adaptation current), but $\delta_{\text{off}}(L) > \delta_{\text{on}}$ for small L (perhaps reflecting that synaptic input decays more slowly than it rises). Our assumption that δ_{off} is a strictly decreasing function of L implies that the fixed point, if it exists, is unique. Suppose now that there is a fixed point L^*. Then

$$g'(L^*) = 1 + \delta'_{\text{off}}(L^*),$$

so, as long as

$$\delta'_{\text{off}}(L^*) > -2,$$

the fixed point will be stable. The condition $\delta'_{\text{off}}(L^*) > -2$ means that δ_{off} is not overly sensitively dependent on L_k.

4.2 Nerve cord simulations

We have performed numerical experiments to illustrate the extent to which our claims have a basis in fact. Since we have simplified Patton's model of a ganglion (Figure 3) by representing it with a single neuron, the term "neuron" or "cell" will be used, but it is implicit that the activity of one of the cells is meant to represent the activity of a ganglion and its influence on the next. Taking a step by step approach, we first tested the slow response of a target neuron to synaptic input.

Suppose the pre-synaptic neuron fires at times kT, $k = 1, 2, 3, \ldots$. Suppose that in the post-synaptic neuron (the target neuron), there is a term of the form

$$I_s = gs(t)(6 - v(t))$$

on the right-hand of the equation governing the membrane potential g, and $s(t)$ jumps up by $\varepsilon_s(1-s)$ each time the pre-synaptic neuron fires, and otherwise decays with time constant $\tau_s > 0$. We made ε small (to achieve slow rise of the excitatory input), and τ_s large (to achieve slow decay). The reversal potential for these excitatory cells is 6. Modeling the post-synaptic neuron as an integrate-and-fire neuron, the equation governing v became

$$
\begin{aligned}
\frac{dv}{dt} &= -\frac{v}{\tau} + gs(t)(6 - v(t)) \quad \text{for } t \neq kT,\ k = 1,2,3,..., \\
\frac{ds}{dt} &= -\frac{s}{\tau_s} \quad \text{for } t \neq kT,\ k = 1,2,3,..., \\
s(kT+0) &= s(kT-0) + \varepsilon(1 - s(kT-0)), \quad k = 1,2,3,..., \\
\text{if } v(t-0) &= 1 \ \text{ then } \ v(t+0) = 0.
\end{aligned}
$$

For the crawling like wave, we predicted that we could only achieve success under specific conditions. The important parameters to consider were the time constants τ_m, τ_s, and τ_w, the synaptic strength g, and the reset values ε_s and ε_w. We concentrated our search of the parameter space on determining appropriate values of τ_s and τ_w, with τ_m =10ms, $g = 0.2$, $\varepsilon_s = 0.003$, and $\varepsilon_w = 0.001$. It was important that τ_m was a reasonable value for an insect interneuron. Heitler et. al. showed that the membrane time constant for neurons in the locust was approximately 10 ms (Heitler et al. 1977) so we chose $\tau_m = 10$ for our LIF neurons. We predicted that we needed persistent neurotransmitter presence and long lasting adaptation so that it would not saturate if the neuron fired for slightly longer than the stable burst duration. We believed that these conditions would allow us to find L^* such that $g'(L^*) = 1 + \delta'_{\text{off}}(L^*)$.

With these parameter values, if a neuron, neuron 0, fires with period T =20 ms and this input drove a target neuron we saw a buildup of excitatory input for almost a second before firing in the target starts (Figure 5).

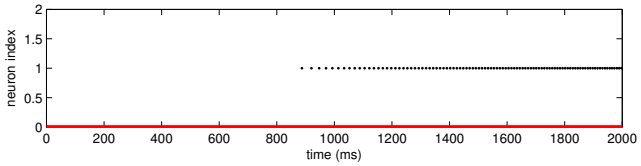

Figure 5: **Onset of firing in target neuron.** Spikes of neuron 1 are represented temporally in the graph above. Neuron 1 receives tonic input from the pre-synaptic cell firing with T =20ms (represented by the red bar along the horizontal axis). The LIF model is used without adaptation and with parameter values $\tau = 10$, $g = 0.2$, $\varepsilon_s = 0.003$, and $\tau_s = 2000$.

With the same parameters as above, we then experimented with the offset of firing within neuron $k+1$ after its presynaptic drive had ceased. First, experiments were performed without adaptation. Based on the abstract overview, we expected $\delta_{\text{off,k+1}}$ to be an increasing function of L_k in this situation. We found this to be the case (Figure 6 A). Second, adaptation was added to the model, with τ_w = 8000 ms and $\varepsilon_w = 0.001$. Here we hoped that $\delta_{\text{off,k+1}}$ would be a decreasing function of L_k so that it would be possible for our mapping from L_k to L_{k+1} to have a stable fixed point. We found that $\delta_{\text{off,k+1}}$ was a decreasing function of L_k in this second situation (Figure 6 B).

Activity was simulated within a linear chain of $n = 20$ cells identical to those used in the

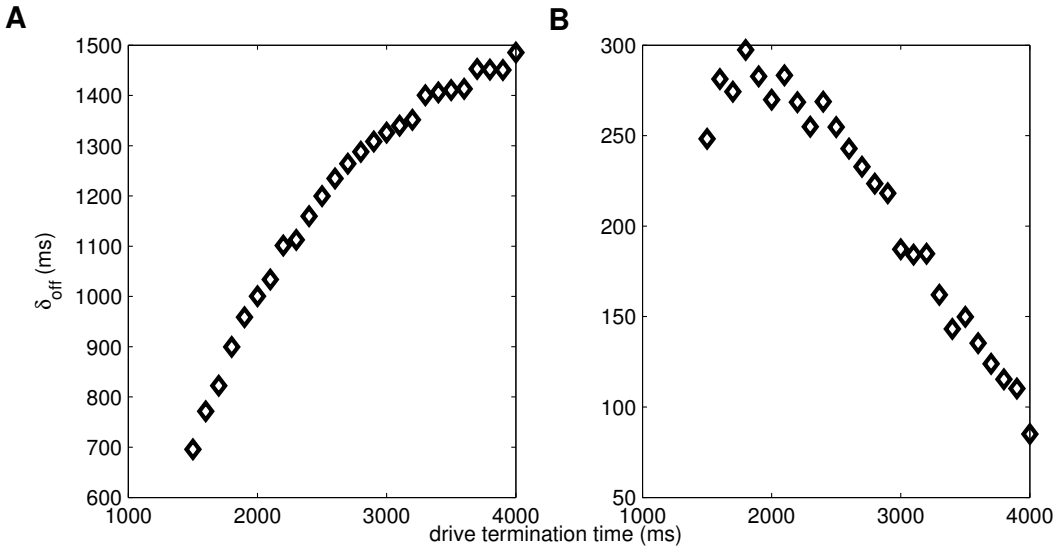

Figure 6: **Offset of firing in ganglion $k+1$ versus drive time (L_k) with and without adaptation.** Ganglion $k+1$ is modeled as a LIF neuron with parameter values $\tau = 10$, $g = 0.2$, $\varepsilon_s = 0.003$, and $\tau_s = 2000$. Plotted is δ_{off} versus input drive time (L_k) for ganglion $k+1$ before (**A**) and after (**B**) adaptation was added to the model with $\tau_w = 8000$ms and $\varepsilon_w = 0.001$.

previous simulations. The cells synapsed anteriorly, as in the circular network design, however the *n*-th was not connected back to drive the first cell. Under these conditions, an anterior grade wave of bursting propagated all the way to the end of the chain of simulated neurons and the duration of bursting within the neurons converged (Figure 7). The pattern was produced in conditions where cell 1 was driven for a time t_d regardless of whether t_d was greater or less than the stable burst duration (Figure 7 A v. B). The stable burst duration for one wave of the pattern is the duration of the burst in cell k once this quantity has reached its steady state. We also found that activity propagates up the chain even if the adaptation parameter is not included in the model, but that the burst duration does not converge (Figure 7 C).

To achieve our total simulation goal of seeing the pattern repeat after drive has ceased, we closed the connection of the linear chain to make it circular. The simulation was run under the condition that after the 0-th neuron ceased to drive the first, the *n*-th neuron was able to drive it. Under these conditions we still saw the wave of bursting travel down the entirety of the nerve cord, but we do not see the wave complete the journey a second time (Figure 8 A & B). The second time that neurons burst, the burst durations decrease increasingly with k. We thought that this could be because there was still too much adaptation in the k-th neuron to allow it to fire enough, or frequently enough to propel equivalent activity into the $k+1$-st neuron. To test this, we experimented with values of τ_w. We saw that the pattern could in fact propagate slightly farther up the nerve cord on the second pass with τ_w =5000ms (Figure 8 B) as opposed to τ_w =8000ms (Figure 8 A). Also, if n was increased the number of neurons that did fire during the second wave increased (unprinted observation). This is congruent with the idea that τ_w is too large because with more cells, each cell would be quiet for a longer period of time before it

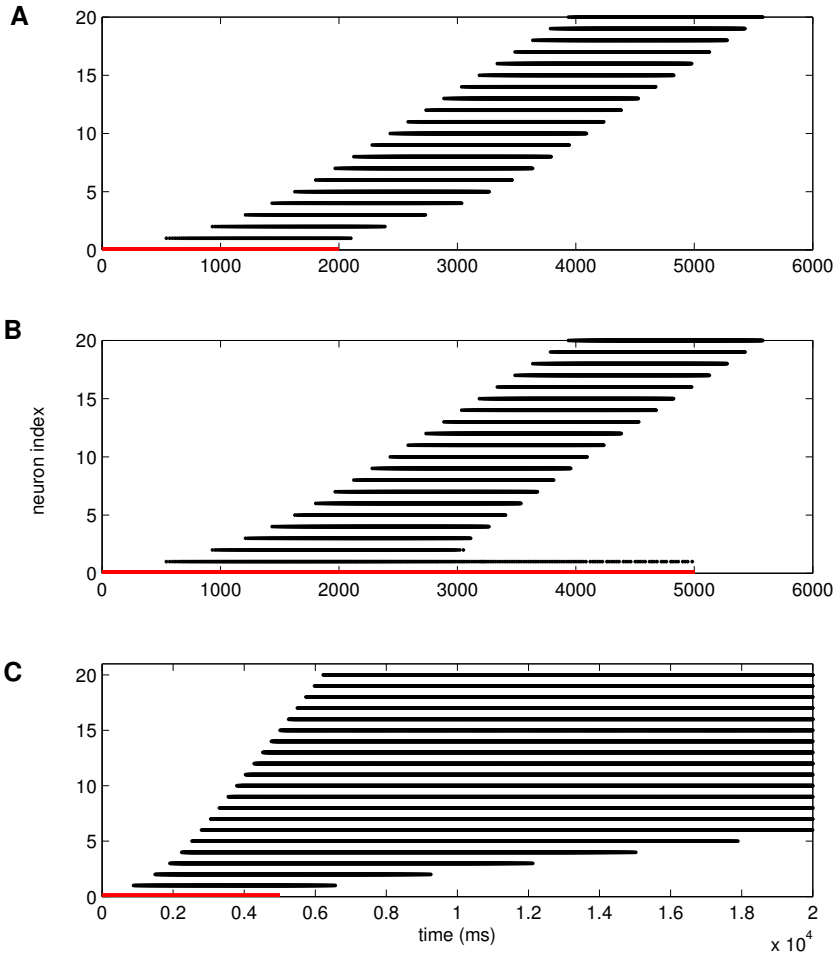

Figure 7: **Firing propagates down a linear chain of $n = 20$ LIF neurons.** The n LIF neurons are identical with $\tau = 10\,\text{ms}$, $\tau_w = 8000\,\text{ms}$, and $\varepsilon_w = 0.001$. The chain of LIF neurons are all connected identically with τ_s =2000ms, $\varepsilon_s = 0.003$, and $g = 0.2$. We call the chain "linear" because neuron n is not connected to drive neuron 1. Again, neuron 0 drives neuron 1 with $T = 20$ starting at $t = 0$ (represented by the red bars on the horizontal axes). **A)** Drive ceases at t =2000 ms. **B)** Drive ceases at t =5000 ms. **C)** Again, drive ceases at t =2000 ms, but in this simulation adaptation has been removed from the LIF model for all n cells.

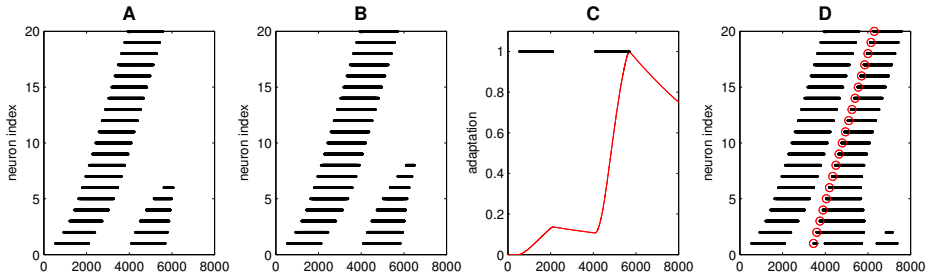

Figure 8: **Propagating wave pattern fails to travel continuously around a circular chain of $n = 20$ LIF neurons.** A uni-directionally connected circular chain of LIF neurons with $\tau = 10$, $g = 0.2$, $\varepsilon_s = 0.003$, $\tau_s = 2000$, and $\varepsilon_w = 0.001$. Neuron 1 was driven until t =2000 ms by neuron 0 firing with period $T = 20$. **A)** TSimulation results with τ_w = 8000 ms. **B)**, and the bottom graph shows τ_w = 5000 ms. **C)** Adaptation w for neuron 1 with τ_w = 8000 ms is plotted and accompanied by the firings of the neuron. Note that w does not decay back to zero by the time neuron 1 begins to fire its second burst. **D)** For this experiment, a simulation that was run to create this plots is identical to the corresponding simulation in **A** except that at the arbitrary time $t = 3300 + 150n$ the adaptation was removed by setting $w = 0$. Simulations similar to that in **B** were also run as a part of this experiment with similar results.

was driven to fire again, allowing its adaptation to decay more. This would allow the pattern to propagate farther up the nerve cord.

We also performed an experiment where all adaptation was removed by setting $w = 0$ for each neuron at a time $t = 3300 + 150n$ (Figure 8 D). This time was chosen because it occurred after the first wave of bursting had ceased in each cell and before the second was expected to start. This start time was estimated by observation of a line with the same slope as the offset of the bursting of the first wave drawn that intersected the linear representation of the first neuron where its activity started on the second pass of activity up the nerve cord. As shown in Figure 8 D, with the arbitrary removal of built up adaptation, the bursting pattern was able to travel up the entirety of the nerve cord a second time. This provided further evidence that adaptation was persisting for too long. Also, if n was increased the number of neurons that did fire during the second wave increased. This is also congruent with the idea that τ_w is too large because with more cells each cell would be silent for longer before it was driven to fire again and so its adaptation would have decayed more. This would allow the pattern to propagate farther up the nerve cord.

However, with τ_w =3000 ms the wave of bursting propagates around the circular chain continuously with stable burst duration (Figure 9). This is confirmed in Figure 9 A for a network where neuron 1 was driven until t =2000 ms by neuron 0 firing with period $T = 20$. In order to verify that the burst duration would still converge with a drive time longer than the stable burst duration, we drove the first cell for 5000 ms. In this case the pattern did not propagate (Figure 9 C). We believe this is because the first cell was still receiving external drive when the last cell started to give it input. This caused the value of w to be larger than if the first neuron were quiet, and therefore firing stopped more quickly just as was seen when τ_w was too large. We did find that driving the first cell for 3000 ms was enough for the drive time to be longer than the stable

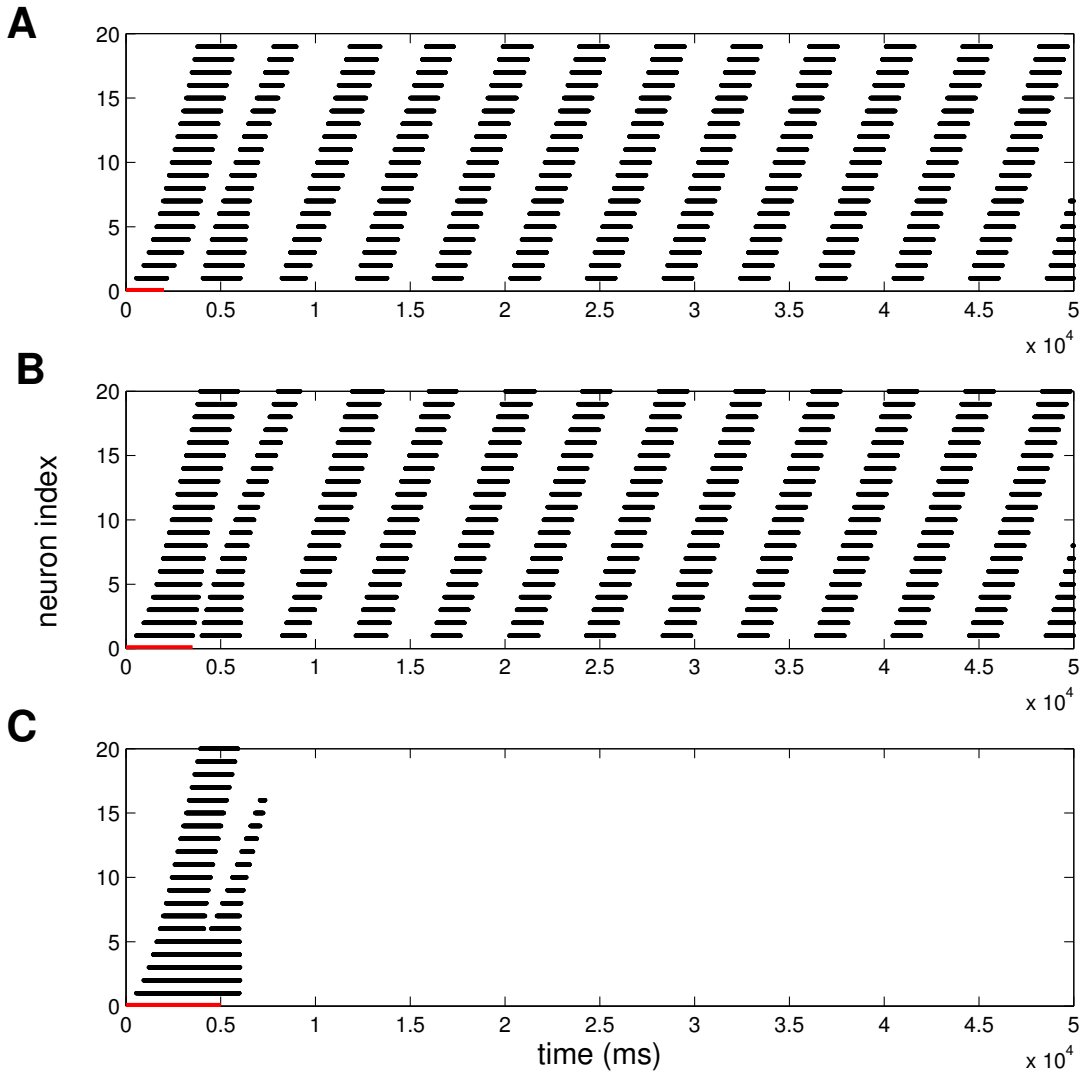

Figure 9: **Decreasing τ_w allows the propagating wave pattern to continue indefinitely within the circular chain of bursters.** The uni-directionally connected circular chain of LIF neurons with $\tau = 10$, $g = 0.2$, $\varepsilon_s = 0.003$, $\tau_s = 2000$, and $\varepsilon_w = 0.001$ was again used in these simulations. Neurons $1, \ldots, n$ had $\tau_w = 3000$ms. The red bars on the horizontal axes denote the time during which neuron 1 was driven by the activity of neuron 0 firing with period $T = 20$. **A)** Neuron 1 was driven until t =2000ms by neuron 0. **B)** Neuron 1 was driven until t =3000ms by neuron 0. **C)** Neuron 1 was driven until t =5000ms by neuron 0. After this the cells were driven by the activity of neuron n in each of the three simulations.

burst duration but not too long for the first cell to stop firing before it was again driven by the last cell (Figure 9 B).

Thus, as we saw with the linear chain of bursters, the pattern is convergent if the cell is driven for a time

$$t \in (L_\infty - \delta,\ L_\infty + \delta)$$

where L_∞ is the stable burst duration and δ is a bound on half the length of the acceptable range for the time t. We note that we have no confirmation that this encompasses all functional drive times, just that there does exist an interval on both sides of the stable burst duration from which drive times can be drawn.

5 Adaptation current enables laterally synchronous and anti-synchronous output within the same network

In the last section we explored a mechanism that allowed for the slow wave of the crawling pattern to propagate along the nerve cord. Next, we needed to test the capabilities of a network modeling just one ganglion to see how both a crawling-like and a casting-like pattern could be elicited. We simplified Patton's model (Figure 3) and represented a ganglion as a laterally inhibitory network of identical ML neurons (Figure 10). A pattern within this network where both sides of the ganglion fire together is crawling-like, because both sides of the animal are active together during crawling in *Manduca*. A casting-like pattern has anti-synchronous activity of the two sides of the ganglion, which reflects how one side of the body wall muscles are driven at a time as the body of the caterpillar moves back and forth.

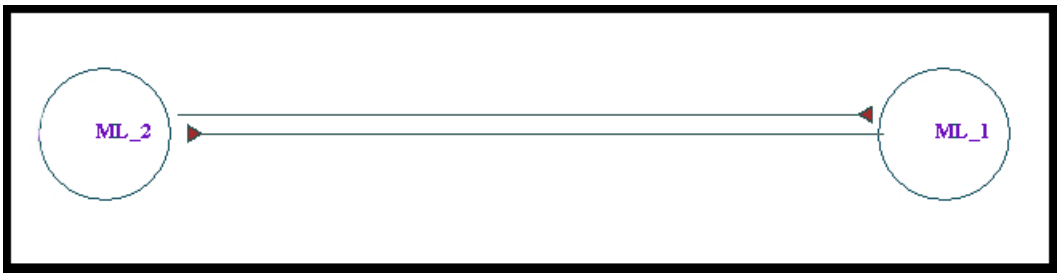

Figure 10: **Network of laterally inhibitory Morris–Lecar neurons.** ML_1 and ML_2 are governed by identical copies of the Morris–Lecar equations for modeling neurons with Ca^{2+} driven spikes and Ca^{2+} gated K^+ adaptation currents. The horizontal lines show the connectivity of the network. The maroon triangles represent inhibitory synapses.

In these experiments, we were able to use Morris-Lecar neurons in place of LIF neurons. As will be discussed, the two experimental networks in this study will need to be combined into one and simulated using a biologically accurate neuron model. Morris-Lecar neurons are more biologically accurate than LIF neurons so simulating with them brings us closer to our eventual goal.

5.1 Abstract overview

In order to see whether a single network could produce two types of output with changing initial conditions, rather than changing parameter values, we varied the drive to one neuron for a short time, while keeping the drive to the other constant. Although both neurons started at an the same initial membrane potential at time zero, if the time after which the first neuron received different drive from the second, call it t_0, is considered to be the beginning of the experiment, we then have two identically driven neurons starting from different initial conditions.

We hypothesize that if adaptation is added to our network, we will see a laterally anti-synchronous activity pattern instead of just one cell inhibiting the other when the two cells start from different initial conditions. We chose a calcium gated potassium current for adaptation. Since ML neurons have calcium spikes, each time a spike is fired the concentration of calcium ions within the cell rises. If we gate a potassium current with calcium, the more spikes that occur, the more likely the membrane will be to hyper-polarize (the effect of allowing potassium to flow across the membrane out of the cell). The idea was that, one cell would until it is inhibited by it's own adaptation current. This would allow the other cell to fire, which in turn would inhibit the first cell from starting to fire once the concentration of calcium inside its membrane had decayed away. Then this process would repeat itself and we would see an alternating pattern.

5.2 Intra-ganglionic simulations

The network simulations were set up and run in SNNAP (©1993-2003 The University of Texas Health Science Center at Houston, Houston TX, http://snnap.uth.tmc.edu).

If both neurons did not have adaptation currents we found that they fired in synchrony when they were driven equally and had identical initial conditions (Figure 11 A). If the two neurons were instead initialized differently by giving one neuron more drive for a brief period at the beginning of the simulation, that neuron would fire rapidly and it's activity would suppress activity of the other (Figure 11 C). These simulations were run with the parameter values spelled out in section 3.2 and experiments were performed to determine appropriate drive magnitudes. If the cells are driven to hard they undergo depolarization block, where the input drive holds the membrane potential above the threshold of the membrane, preventing the cell from firing. If the difference in initial conditions is not great enough, but also not zero, then neither cell fires for the duration of the 3 second simulation. When the two cells were driven equally they received $2\mu A$ of current. When the two cells had different initial conditions they were each given $1.9\mu A$ of current, and one received an extra $0.15\mu A$ for the first $0.2sec$ of the 3 second simulation.

If both neurons did have adaptation currents we found that they fired in synchrony when they were driven equally and had identical initial conditions (Figure 11 B). The frequency of firing of the neurons with adaptation and higher drive was higher than that of the network without

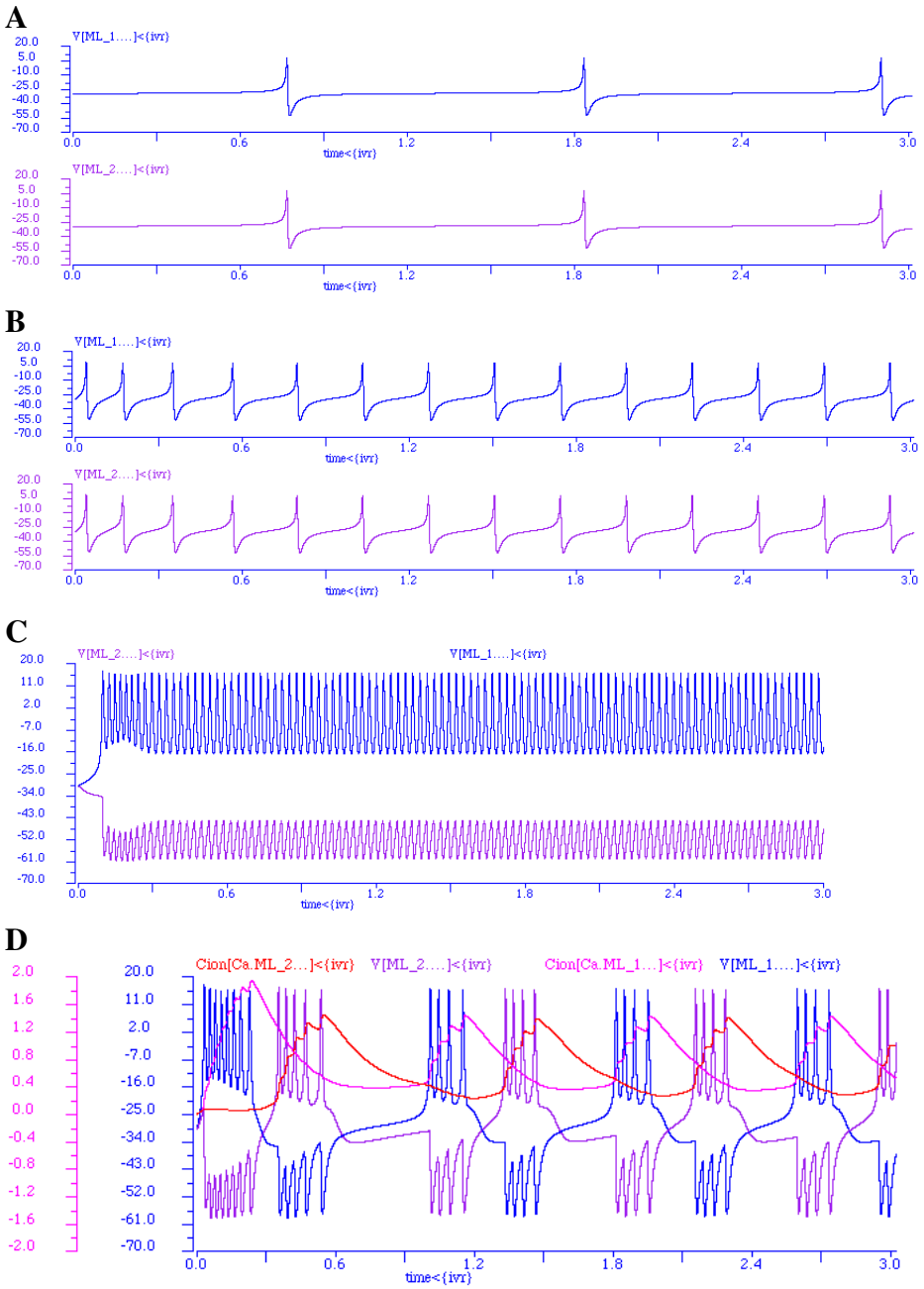

Figure 11: **Adaptation enables anti-synchrony in a laterally inhibitory network of Morris-Lecar neurons.** Activity of the two neurons started from identical initial conditions is shown in panels **A** and **B**. **A)** (No Adaptation) Both cells receive $I = 2\mu A$ for the duration of the simulation. **B)** (Adaptation Included) Both cells receive $I = 2.25\mu A$ for the duration of the simulation. In the presence or absence of adaptation, when ML_1 and ML_2 have identical initial conditions and drive they fire in synchrony. Activity of the two neurons where one initially receives elevated drive is shown in panels **C** and **D**. **C)** (No Adaptation) Both cells receive $I = 1.9\mu A$ for the duration of the simulation, but ML_1 receives an extra $I' = 0.15\mu A$ for the first 0.2 seconds. **D)** (Adaptation Included) Both cells receive $I = 2.2\mu A$ for the duration of the simulation, but ML_1 receives an extra $I' = 0.2\mu A$ for the first 0.2 seconds. Always ML_1 is shown in blue and ML_2 in purple. In panel **D** the magenta (ML_1) and red (ML_2) curves represent the concentration of calcium inside the cell.

adaptation and lower drive. If instead one of the adaptive neurons initially receives extra drive, we found that the network did in fact produce an anti-synchronous and repetitive activity pattern (Figure 11 D). These simulations were also run with the parameter values spelled out in section 3.2 and experiments were performed to determine appropriate drive magnitudes. We started our search at the value given in the SNNAP tutorial manual (snn 2003, Ch. 4). When the two cells were driven equally they received $2.25\mu A$ of current. When the two cells had different initial conditions they were each given $2.2\mu A$ of current, but one received an extra $0.2\mu A$ for the first 0.2 of the 3 second simulation. The adaptive network could take in higher drive and fire at higher frequency. In this range it seems that the added adaptation prevented the cells from experiencing depolarization block at the higher frequency. When driven at just $2\mu A$ the adaptive cells were silent independent of the difference between their initial conditions. When the cells with adaptation are driven further, they do experience depolarization block just as the non-adaptive cells did. This suggests that adding adaptation raises the range of amperages that will elicit fining in the cell and also enables the anti-synchronous pattern.

6 Discussion

Our study can be summed up into two major findings. First, that adaptation is necessary for a slow wave of bursting to propagate around our nerve cord. Second, that adaptation is necessary for anti-synchronous activity within our ganglion.

Our hypotheses about the parameter values for our LIF nerve cord simulations proved correct. Adaptation is required for the slow pattern to propagate continuously around the nerve cord. With time constants τ_m =10ms, τ_s =2000ms, and τ_w =3000ms we are able to achieve the desired results within a network of 20 ganglia. The adaptation is not as persistent as we originally thought it needed to be. For a network with $n \neq 20$ a convergent circular chain system would be expected to have different parameter values. We also found that the forward propagating wave is robust and occurs for different initial drive times, within a certain range around the stable burst duration.

In the future, it would be very interesting to explicitly develop two mappings: one from the parameter values to the stable burst duration for the first wave up the nerve cord, and a second from that stable burst duration to the final stable burst duration. As you can see in figure 9 A and B the final stable burst duration is shorter than the first wave of bursts. It would be interesting to examine the frequency of firing within the bursts and experiment to determine how it effects the stable burst duration. We could use this information to tweak the timing of our pattern in order to make it as representative of crawling in *Manduca* as possible.

It could be argued that the design of the crawling pattern is not the most biologically accurate. To this, we can only say that we chose one approach to a crawling pattern and then found out how to make it work. An extension of this study could branch further into making

the model for the pattern more accurate, and then reproducing the process we have undertaken beginning from a different set of assumptions. The first aspect that it would be important to examine is whether the pattern originates from a network that is constantly driven, or one that only requires an initial drive for the crawling pattern to propagate (like ours). s Greater biological accuracy, though not necessary for our purposes, is always advantageous because it will allow us to more easily incorporate more facets of the living system into our model. However, models get complicated quickly, and it is best to not try to incorporate anything into a model if its purpose or function are not completely understood. We kept our model simple and found one plausible mechanism through which a crawling like-pattern can be produced. Since we are not entirely sure of what happens within the CNS of *Manduca* or similar organisms, we feel confident keeping our results more abstract so that we avoid making claims that we are not sure of. Our results could be incorporated into a caterpillar model robot to control its crawling.

For the intra-ganglionic simulations of the crawling-like or casting-like patterns (Section 5) we also achieved our results under a specific set of parameter values. For these neurons there was less experimentation to find the parameter values because we had success early on with values form a model that we borrowed from the software. Our result that both synchronous and anti-synchronous activity within a laterally inhibitory network can be achieved by incorporating adaptation currents into the two neurons provides evidence that it would be possible for one network architecture to produce both crawling and casting within *Manduca*, and even stronger evidence that one could incorporate only one network into a biomimetic robot to control both behaviors.

The first step towards controlling both behaviors in a biomimetic unit in this way is to combine our two simulations. We would need to numerically show that the two patterns could be produced by the combined network before it was reasonable to try and produce some physical network that could be implanted into a robot. When our two networks are combined both patterns will be produced by activity in the same cells, so before we can even combine the two it would be advantageous to show that we can achieve the results that we have achieved in this study where both simulations are run on the same type of neurons.

Now that we know both outcomes are attainable, it is time to start working towards more accurate representations of the crawling pattern. In terms of LIF or ML neurons, we know that ML neurons are more biologically accurate. Thus, it would first make sense to try to elicit the slow forward propagating wave within a nerve cord of ML neurons. Next the two network designs would need to be combined. When combined the ganglia would probably resemble Pattons network almost exactly and we would have to decide between contra or ipsilateral excitation from one ganglion to the next.

It would be very valuable to develop a minimal cell model for *Manduca*, or at least for an insect cell. In his 1991 work, Av Ron created a minimal cell model of the lobster cell working from models of the squid giant axon (Av-Ron et al. 1991). He detailed his process, and it would be possible to extend his work for a manduca cell model. Recordings from single neurons in

the CNS of *Manduca* and related organisms and a good amount of time would be necessary.

Acknowledgements

I would like to thank,

Professor B. Trimmer and Professor C. Börgers for their help and advice on this project and throughout my Tufts career. My extremely unique experience would not have been possible without either of these two individuals, and for this I will forever be thankful. I would also like to thank members of Tufts Neuromechanics and Biomimetic Devices lab Cinzia Metallo, William A. Woods Jr., Emily Pitcairn, and Vishesh Vikas for helping her get started in research, answering questions, teaching, and providing a friendly lab environment for me to work in. Finally, thank you to my friends and family for their support and encouragement along the way, and the Tufts Center for Interdisciplinary Studies for accepting my proposal to major in Mathematical Neurobiology.

References

(2003). *Tutorial Manual for Version 8 of SNNAP*. The University of Texas–Houston Medical School, Center for Computational Biomedicine, Department of Neurobiology and Anatomy, Houston, TX 77030.

Av-Ron, E., Parnas, H., and Segel, L. A. (1991). A minimal biophysical model for an excitable and oscillatory neuron. *Biol. Cybern.*, 65:487–500.

Cohen, A. H. and Harris-Warrick, R. M. (1984). Strychnine eliminates alternating motor output during fictive locomotion in the lamprey. *Brain Research*, 293:164–167.

Delcomyn, F. (1980). Neural basis of rhythmic behavior in animals. *Science*, 210(13):492–498.

Getting, P. A. (1981). Mechanisms of pattern generation underlying swimming in *Tritonia*. i. neuronal network formed by monosynaptic connections. *Journal of Neurophysiology*, 46(1):65–79.

Gorczyca, M. G., Budnik, V., White, K., and Wu, C. F. (1991). Dual muscarinic and nicotinic action on a motor program in *Drosophila*. *Journal of Neurobiology*, 22(4):391–404.

Heitler, W. J., Goodman, C. S., and Fraser Rowell, C. F. (1977). The effects of temperature on the threshold of identified neurons in the locust. *J. comp. Physiol.*, 117:163–182.

Hodgkin, A. L. and Huxley, A. F. (1952). A quantitative description of membrane current and its application to conduction and excitation in the nerve. *J. Physiol.*, 117:500–544.

Johnston, R. M., Consoulas, C., Pfluger, H. J., and Levine, R. B. (1998). Patterned activation of unpaired median neurons during fictive crawling in *Manduca sexta* larvae. *The Journal of Experimental Biology*, 202:103–113.

Johnston, R. M. and Levine, R. B. (1996). Crawling motor patterns induced by pilocarpine in isolated larval nerve cords of *Manduca sexta*. *The Journal of Neurophysiology*, 76:3178–3195.

Johnston, R. M. and Levine, R. B. (2002). Thoracic leg motoneruons in the isolated cns of adult *Manduca* produce patterned activity in response to pilocarpine, which is distinct from that produced in larvae. *Invertibrate Neuroscience*, 4:175–192.

Kien, J. (1983). The initiation and maintenance of walking in the locust: an alternative to the command concept. *Proc. R. Soc. Lond. B*, 219:137–174.

Lajoie, G. and Shea-Brown, E. (2011). Shared inputs, entrainment, and desynchrony in elliptic bursters: from slow passage to discontinuous circle maps. *SIAM J. Appl. Dyn. Syst.*, 10(4):1232–1271.

Lane, N. J. (1972). Fine structure of a lepidopteran nervous system and its accessibility to peroxidase and lanthanum. *Z. Zellforsch*, 131:205 – 222.

Levine, R. B. and Truman, J. W. (1985). Dendritic reorganization of abdominal motoneurons during metamorphosis of the moth, *Manduca sexta*. *The Journal of Neuroscience*, 5(9):2424–2431.

Mezoff, S., Papastathis, N., Takesian, A., and Trimmer, B. A. (2004). The biomechanical and neural control of hydrostatic limb movements in *Manduca Sexta*. *The Journal of Experimental Biology*, 207:3043–3053.

Morris, C. and Lecar, H. (1981). Voltage oscillations in the barnacle giant muscle fiber. *Biophys. J.*, 35:193–213.

Morris, C. E. (1984). Electrophysiological effects of cholinergic agents on the cns of a nicotine-resistant insect, the tobacco hornworm (*Manduca sexta*). *The Journal of Experimental Zoology*, 229:361 –374.

Novicki, A. and Weeks, J. C. (1995). A single pair of interneurons controls motor neuron activity during pre–exdysis compression behavior in larval *Manduca sexta*. *J Comp Physiol A*, 176:45–54.

Patton, J. (2000). Pilocarpine induces a novel motor rhythm in addition to fictive crawling in isolated nerve cords of larval *Manduca sexta*. Technical report, Tufts University. Department of Biology Senior Thesis.

Pfeifer, R. and Bongard, J. (2007). *How The Body Shapes The Way We Think*. The MIT Press.

Pichon, Y., Sattelle, D. B., and Lane, N. J. (1972). Conduction processes in the nerve cord of the moth *Manduca sexta* in relation to its ultrastructure and haemolymph ionic composition. *J. Exp. Biol.*, 56:717 – 734.

Rohrbacher, J. (1994). Fictive chewing activity in the motor neurons and interneurons of the subesophageal ganglion of *Manduca sexta* larvae. *J Comp Physiol A*, 175:629–637.

Ryckebusch, S. and Laurent, G. (1993). Rhythmic patterns evoked in the locust leg motor neurons by the muscarinic agonist pilocarpine. *Journal of Neurophysiology*, 69(5):1583–1595.

Sandstrom, D. J. and Weeks, J. C. (1991). Reidentification of larval interneurons in the pupal stage of the tobacco hornworm, *Manduca sexta*. *The Journal of Comparative Neurology*, 308:311–327.

Selverston, A. I., King, D. G., Russell, D. F., and Miller, J. P. (1976). The stomatogastric nervous system: structure and function of a small neural network. *Prog. Neurobiol.*, 7(2):15–290.

Simon, M. A., Fusillo, S. J., Colman, K., and Trimmer, B. A. (2010). Motor patterns associated with crawling in a soft-bodied arthropod. *The Journal of Experimental Biology*, 213:2303–2309.

Torre, V. and Poggio, T. (1978). A synaptic mechanism possibly underlying directional selectivity to motion. *Prec. R. Soc. Lond. B*, 202:409–416.

Trimmer, B. A. (1994). Characterization of a muscarinic current that regulates excitability of and identified insect motoneuron. *Journal of Neurophysiology*, 72(4):1862–1873.

Trimmer, B. A. (1995). Current excitement from insect muscarinic receptors. *TINS*, 18(2):104–111.

Trimmer, B. A. and Weeks, J. C. (1993). Muscarinic acetylcholine receptors modulate the excitability of an identified insect motoneuron. *Journal of Neurophysiology*, 69(6):1821–1836.

Waldrop, B. and Levine, R. B. (1992). Intersegmental interneurons serving larval and pupal mechanosensory reflexes in the moth *Manduca sexta*. *J Comp Physiol A*, 171:195–205.

Weeks, J. C. and Jacobs, G. A. (1987). A reflex behavior mediated by monosynaptic connections between hair afferents and motoneurons in the larval tobacco hornworm, *Manduca sexta*. *J Comp Physiol A*, 160:315–329.

Weeks, J. C. and Truman, J. W. (1984). Neural organization of peptide–activated ecdysis behaviors during the metamorphosis of *Manduca sexta*. *J Comp Physiol A*, 155:407–422.